Biochimica et Biophysica Acta, 1017 (1990) 49–56
Elsevier

BBABIO 43206

The structure of spinach Photosystem I studied by electron microscopy

Egbert J. Boekema [1], R. Max Wynn [2,*] and Richard Malkin [2]

[1] *Biochemisch Laboratorium, Rijksuniversiteit Groningen, Groningen (The Netherlands)* [2] *Department of Plant Biology, University of California, Berkeley, CA (U.S.A.)*

(Received 27 October 1989)

Key words: Photosystem I structure; Electron microscopy; Image analysis; (Spinach)

The structure of three types of Photosystem I (PS I) complex isolated from spinach chloroplasts was studied by electron microscopy and computer image analysis. Molecular projections (top views and side views) of a native PS I complex (PSI-200), an antenna-depleted PS I complex (PSI-100) and the PS I reaction center complex (CPI) were analyzed. The overall structure of the native PS I complex was found to be a disk with dimensions (corrected for attached detergent) of 16 × 12 nm in the plane of the membrane and a height of 6.8 nm. The PSI-100 and CPI complexes gave much smaller projections but these were similar in shape and size to those of the previously analyzed cyanobacterial PS I complex. The arrangement of the subunits within the native PS I complex is discussed. It is concluded that a shell of about eight light-harvesting complex (LHCI) subunits attached to the PSI-100 complex fits the dimensions and shape of the PSI-200 complex.

Introduction

The Photosystem I (PS I) complex catalyzes a light-dependent transfer of electrons from reduced plastocyanin to ferredoxin. In the light, a photoinduced charge separation in the reaction center yields an oxidation of a special chlorophyll *a* molecule, P-700, and the sequential reduction of a number of bound electron acceptors (see Refs. 1 and 2 for recent reviews).

The PS I complex contains two high molecular mass subunits, the products of the *psaA* and *psaB* genes [3,4], and numerous low molecular mass subunits. Amino-acid sequences derived from DNA sequences of many of these subunits are now available [5–9], although a functional role for some of these subunits has not been defined.

The overall structure of the PS I core complex has been studied by electron microscopy. Boekema et al. [10,11] analyzed isolated PS I particles from the cyanobacterium *Synechococcus* sp. prepared in the detergents octyl glucoside and/or dodecyl maltoside. A disk-like particle of about 19 × 6.5 nm consisting of three monomers was found. Ford et al. [12] observed a very similar trimeric structure from another thermophilic cyanobacterium. The monomeric reaction centers measure about 9–10 × 15 nm in both cases [12,13], or 7 × 12 nm after correction for attached detergent. It is unlikely that the trimeric particles exist in vivo as well, but for some special thermophilic cyanobacteria this possibility can not be excluded at the moment [13].

The shape and dimensions of the native PS I complex from higher plant chloroplasts are less clear. From freeze-fracture studies it was concluded that monomeric reaction center particles (7–10 nm) associate with specific light-harvesting complex (LHCI) subunits resulting in a spectrum of 10–13 nm particles [14,15]. By comparison of fracture faces of mutant and wild-type barley thylakoid membranes, Simpson found PS I particles with dimensions of 10.3 × 12.3 nm [16]. The freeze-fracture studies are very useful for revealing overall features and numbers of the various thylakoid membrane proteins in vivo, but since the resolution is generally lower than for the negative staining technique, it is difficult to relate particle dimensions obtained from both techniques closely.

In this paper we report on the detailed characterization by electron microscopy of three different preparations from spinach. A model is presented which describes the organization of the subunits of the PS I complex.

* Present address: Department of Biochemistry, University of Texas Medical Center, Dallas, TX, U.S.A.

Correspondence: E.J. Boekema, Biochemisch Laboratorium, Rijksuniversiteit Groningen, Nijenborgh 16, 9747 AG Groningen, The Netherlands.

Materials and Methods

PS I complexes (PSI-200, PSI-100 and CPI) were prepared from spinach chloroplasts as previously described by Wynn and Malkin [17]. Each complex was bound to a TSK-650 DEAE resin and washed with 20 mM Tris-HCl (pH 7.5) and 0.03% dodecyl maltoside to exchange the detergents. Following 10–15 column volumes of wash buffer, the complexes were eluted with the above buffer containing 200 mM NaCl. The PSI-200 contained approx. 200 Chl/P700 while PSI-100 and CPI contained approx. 100 Chl/P700. The latter two preparations contained little or no chlorophyll *b*, while PSI-200 had a Chl *a*/*b* ratio of 5.5. An analysis of the subunit composition of the respective complexes utilizing SDS-PAGE, shown in Fig. 1, confirms the depletion of the light-harvesting chlorophyll protein subunits (molecular masses 24–27 kDa) from PSI-100 and CPI.

Specimens for electron microscopy were prepared by the droplet method, using 1% (w/v) unbuffered uranyl acetate as a negative stain. For electron microscopy the purified PS I samples were diluted in 10 mM Tris-HCl (pH 7.5) plus 0.03% dodecyl maltoside [10]. Electron microscopy was carried out on a Philips EM 400 microscope at 60 000 × magnification In order to allow comparison between the three types of PS I particle, the samples and the electron microscope procedures were standarized as much as possible, for instance by using carbon support films from the same batch.

Selected micrographs were digitized with a Joyce Loebl Scandig 3 rotating-drum densitometer. The scanning step used was 25 μm, corresponding to a pixel size of 0.42 nm in the object. Image analysis was performed by means of IMAGIC software [18–20] on a micro-VAX-II computer. Correspondence analysis and classification [20–22] were performed on the aligned data set in order to obtain an impression of the variation as present in the projections and to discriminate between principal different views.

Results

Previously, it was found that the negative staining technique gives good specimens of photosynthetic complexes for electron microscopy if detergent was added in a concentration of about 2–3-times the critical micellar concentration during preparation [10,11]. Good results were obtained with the detergent dodecyl maltoside. Top- and side-view projections could be easily recognized and evidence was presented that the top views represent the view in the plane of the membrane [11]. Electron micrographs from three types of spinach PS I particle, prepared in a similar way, show clear projections and a low background.

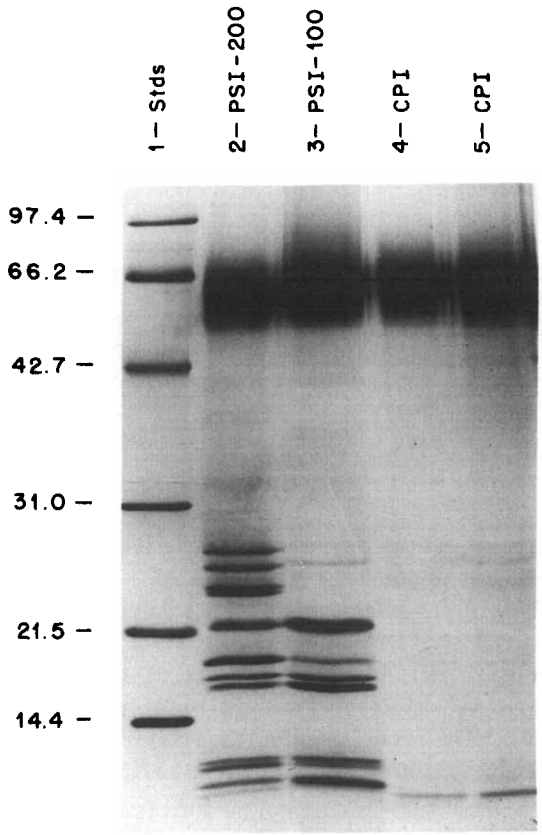

Fig. 1. SDS-PAGE of the PS I preparations, PSI-200, PSI-100 and CPI. Approx. 10 μg of chlorophyll in each complex was used and gels were run as previously described in Ref. 15.

Analysis of CPI projections

Electron micrographs of CPI preparations (Fig. 2) show many top-view projections and some side-view projections; the overall dimensions of CPI are summarized in Table I. The top views are elongated, with a length to width ratio of 1.46. In many cases, the top views are angular and one point is sharper than the other one, resulting in projections similar to those previously observed for cyanobacterial PS I particles [10–12]. Others, however, have a more rounded shape and likely this variance was caused by slight differences in the

TABLE I

Dimensions (nm) of various Photosystem I particles in dodecyl maltoside, measured from top- and side-view projections as seen in the electron microscope

The thickness corresponds to the distance over the membrane in vivo; the length and width are the dimensions in the plane of the membrane, without correction for detergent. Number of measurements between brackets.

	CPI	PSI-100	PSI-200
Length	15.3 ± 0.7 (150)	16.2 ± 1.1 (118)	20.0 ± 1.2 (176)
Width	10.5 ± 0.6 (125)	11.1 ± 0.7 (118)	16.0 ± 1.1 (100)
Thickness	6.3 ± 0.4 (72)	6.9 ± 0.4 (67)	6.8 ± 0.4 (62)

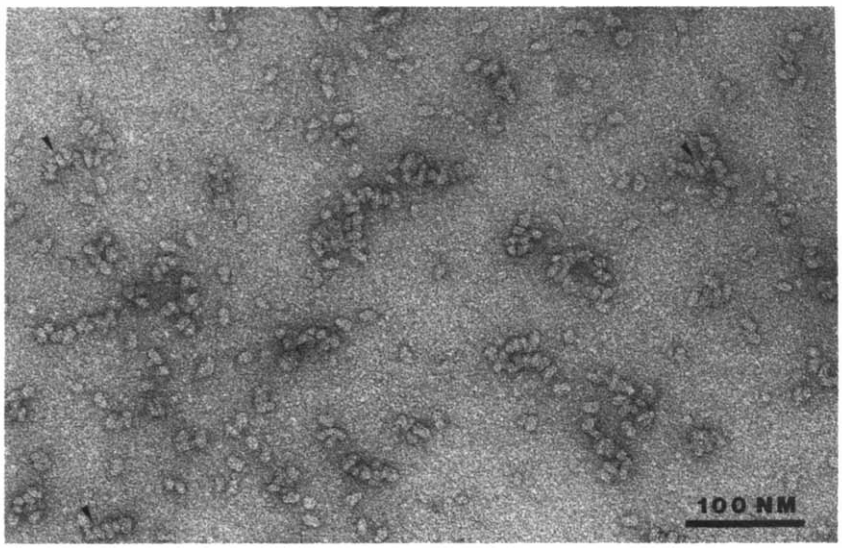

Fig. 2. Electron micrograph of CPI complexes, negatively stained with 1% uranyl acetate in the presence of 0.03% dodecyl maltoside. Some side views have been indicated by arrows.

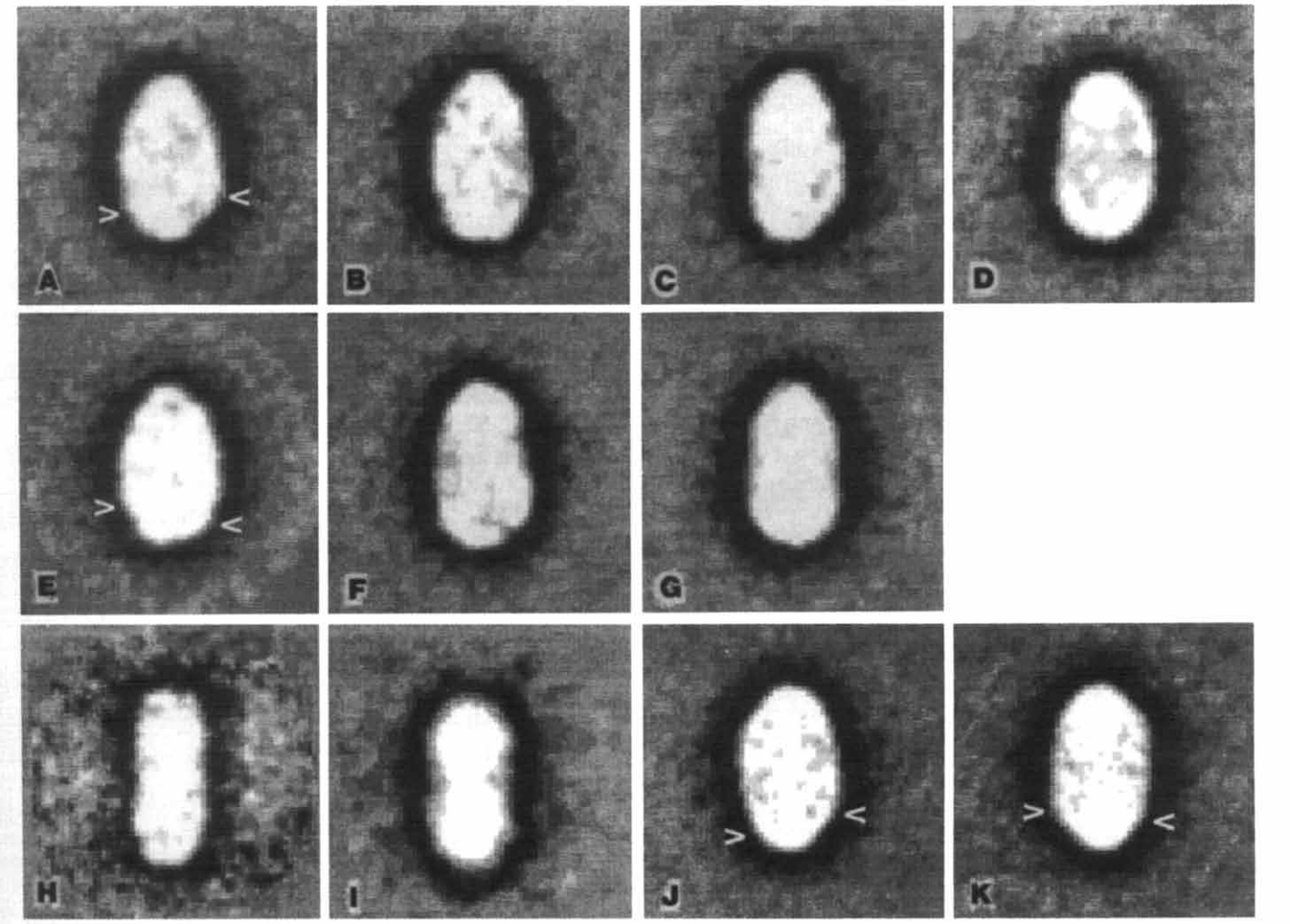

Fig. 3. Image analysis of CPI-projections. (A–G) show the result of correspondence analysis and classification on 812 aligned top view projections. The data set was decomposed into seven classes (A–G) with 109, 108, 87, 108, 95, 110 and 114 projections, respectively. During classification 10% of the projections were automatically rejected. (H) Sum of 42 aligned CPI side-view projections. (I) Sum of 28 projections of particles in a position intermediate between those of (A–G) and (H). (J) and (K) Sums of 118 and 93 projections (out of the 812) showing both types of handedness, on the projections two-fold rotational symmetry has been imposed. The field of one displayed particle is 64×64 pixels or 27×27 nm.

detergent boundary layer and by the low signal-to-noise ratio which is inherent to individual projections.

To gain a further impression of the shape of this minimal particle, image analysis was carried out and 812 top-view projections and 142 side-view projection were selected from six micrographs to ensure good statistical significance of the results. The top-view projections were brought into register by repeated alignments on improving references [19,20]. The CPI projections were often asymmetrical in shape, which means that in principle two groups of projections could be expected, caused by up and down attachment of complexes on the carbon support. This difference in attachment causes a difference in handedness, and previously, for the cyanobacterial trimeric complex [11] the two groups of projections could be separated. For CPI, we also applied multivariate statistical analysis to discriminate between different types of projection. After the correspondence analysis step, the 812 aligned top-view projections were classified into (an arbitrarily chosen number of) 7 classes.

Fig. 3 shows the results of the classification. The classes reflect the variation present in the data set. The main difference was the width of the projections, which varies over about 1 nm between the various classes. This effect became even more apparent if the data set was decomposed in just two classes (not shown). In Fig. 3, classes C, F and G have the smallest width. Small differences in the length (Class E vs. F) also exist. Furthermore, a difference in handedness can be seen: 5A and C are sums of projections of one type and B and E represent the other one. This difference in handedness is, however, not easily recognizable. In Fig. 3J and K, which represent particles with the most extreme angular shape, the handedness is more obvious; both images are clearly mirror-related. These sums were, however, two-fold rotationally averaged, which facilitates the visualization of the handedness.

The asymmetry of CPI is an interesting result by itself. CPI contains one copy of two large subunits with masses of 83 and 82.4 kDa, which run at 62 and 58 kDa on the gel (Fig. 1) with homologies in their amino-acid sequences [3,4]. Therefore, CPI top-view projections with close to two-fold symmetry could be expected, like in Fig. 3J,K where this symmetry was imposed. However, a third small hydrophobic subunit, which runs at 6 kDa on the gel system (Fig. 1) is present in the CPI complexes, and this subunit could cause the asymmetry if binding occurs close to one of the outer points of the projection.

Although the contours are sharp, no clear inner features are recognizable in the top view projections, which is not unexpected since the complexes are very flat particles, as can be seen from the averaged image of the side-view projections (Fig. 3H). There is no indication for the position of the two large subunits of CPI, but projections of particles in intermediate positions (Fig. 3I) show a small cleft half way along the projections, which may be an indication for some separation between both large subunits.

Analysis of PSI-100

In comparison to CPI, the PSI-100 complexes contain single copies of several low-molecular-mass subunits, with masses between 6 and 22 kDa on the gel (Fig. 1), and with calculated masses from the sequence between 8.9 and 17.9 kDa. The PSI-100 top views measure 16.2×11.1 nm (Fig. 4, Table I) and are quite similar to those of CPI, with the same length to width ratio (1.46). However, PSI-100 is slightly larger in all three dimensions (Table I), giving a difference in volume of 23%. The greater length seems to be significant; PSI-100 complexes were also examined previously on a Philips EM 300 microscope (unpublished data), in which case we found an overall length of 15.8 ± 1 nm ($n = 200$). If the dimensions for the top-view projection are corrected for a detergent boundary layer of 1.7 nm [23], the difference is 26%. The difference in mass between CPI and PSI-100 is about 22%, calculated from the total masses of the consisting subunits and pigments (assuming 100 attached chlorophylls binding to the large subunits, and neglecting other pigments and iron-sulfur centers) *. The measured difference in dimensions and the calculated difference in mass are quite similar. From the recently determined sequences of the smaller subunits it is predicted that most of their structures is hydrophilic without membrane spanning α-helices [5–9]. This would explain the smaller thickness of CPI (Table I). However, the projection in the plane (top view) of PSI-100 is slightly but significantly larger than those of CPI and this can only be caused by parts of the structure of the smaller subunits buried in the membrane. This confirms work of Moller and co-workers [24], who recently sequenced a 10.2 kDa polypeptide from barley, which shows one membrane spanning region.

In comparison to CPI, the top view projections of the PSI-100 particles often show a stain accumulation on one side (Fig. 4). This could be caused by differences in height, slight tilts of the molecules on the carbon support or by charge differences on the protein surface. Since the side-view projections show that PSI-100 is a very flat molecule, the latter explanation seems the most plausible one.

* For the calculation of particle masses we took subunit masses (kDa) calculated from the sequences, if available:

CPI	83	82.4		9.7				
PSI-100	83	82.4	8.9	9.7	10.2	10.8	17.3	17.9
PSI-200	83	82.4	8.9	9.7	10.2	10.8	17.3	17.9

plus 96 for 4 LHCI's (26.1 24.9 23 and 22).

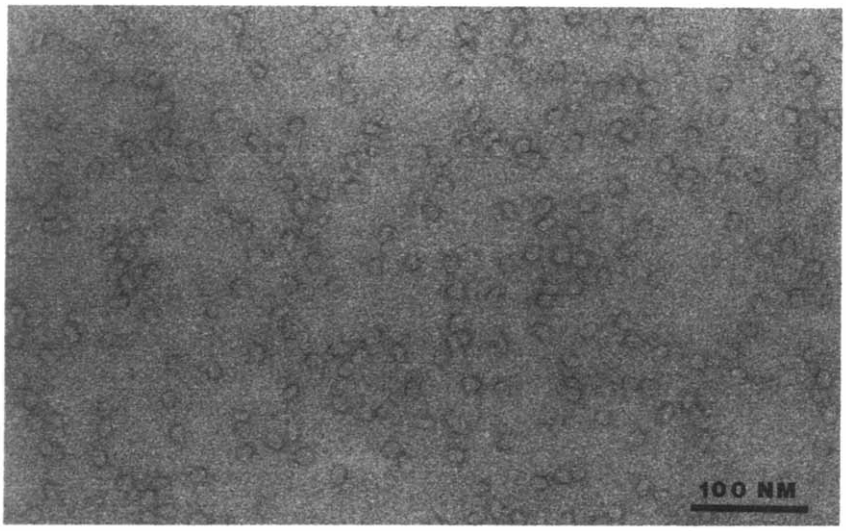

Fig. 4. Electron micrograph of negatively stained PSI-100 complexes.

The dimensions of the PSI-100 complex measured from the top views (16.2 × 11.1 nm) are slightly larger than the ones of the cyanobacterial PS I complex 15.3 × 10.6 nm) [13]. The latter dimensions are, however, derived from image analysis. Dimensions from image analysis are usually a few percent smaller than the ones from direct measurements (see also Discussion). Computer averaging on PSI-100 was not carried out, because of the odd staining behavior, but the dimensions of CPI top views from image analysis (15.2 × 9.7 nm) are slightly smaller than those of PSI-100. This is not unexpected, since the the cyanobacterial PS I complex and PSI-100 have about similar numbers of (smaller) subunits, but CPI lacks five small subunit in comparison to PSI-100.

Analysis of PSI-200

Native PS I particles gave again top- and side-view projections and also intermediate projections of particles in tilted positions (Fig. 5). The population of particles of the PSI-200 preparation is slightly inhomogeneous, which could possibly be explained by differences in the numbers of attached LHCI (light-harvesting complex I) subunits in vivo. It has been found that PS Iα particles, which are located in the grana membrane region, have an antenna size which is 30% larger than those of PS Iβ particles, located in the stroma membrane region [25]. Instability of the isolated PS I particles, resulting in the loss of attached LHCI subunits upon preparation for microscopy, could be another possiblity for the inhomogeneity. Nevertherless,

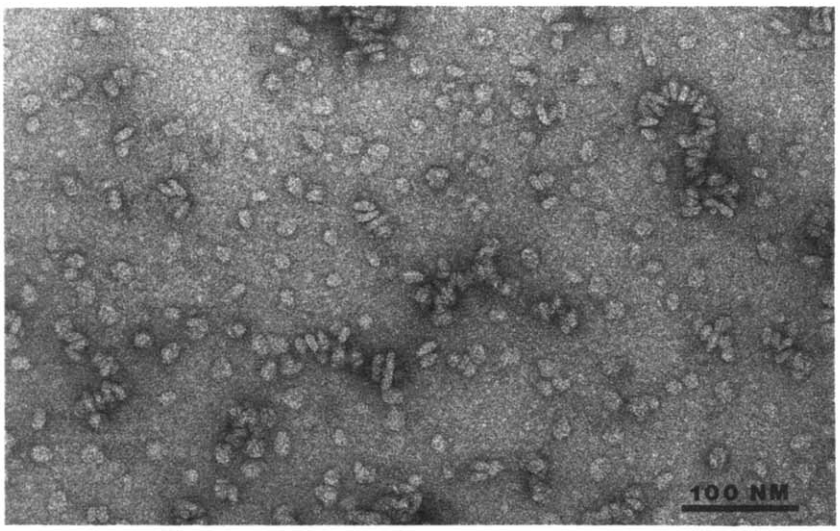

Fig. 5. Electron micrograph of negatively stained PSI-200 complexes.

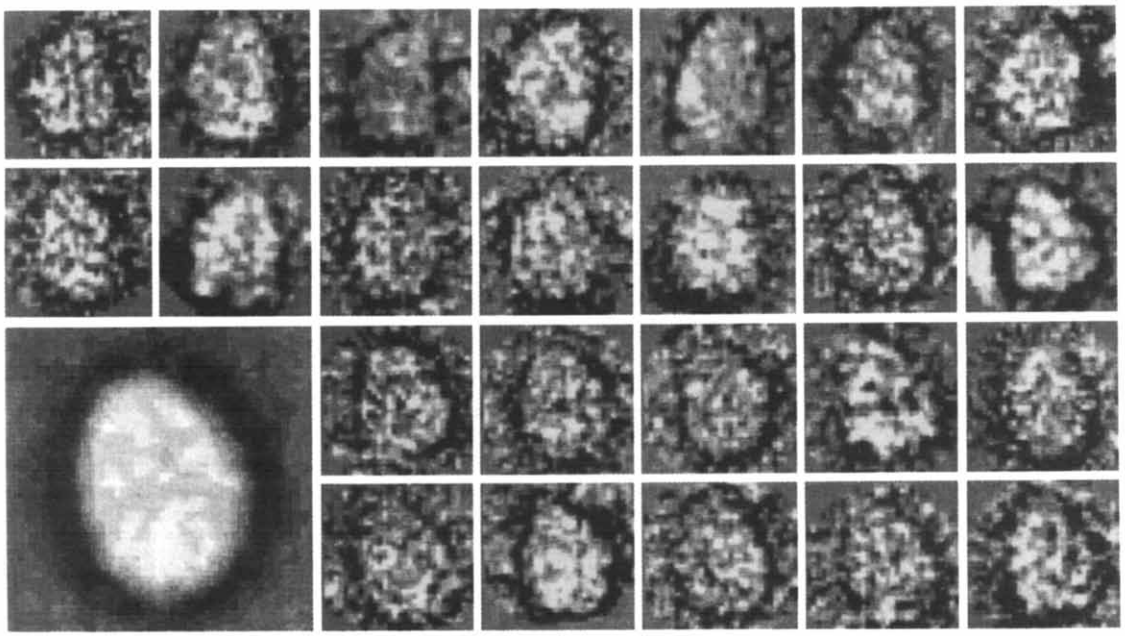

Fig. 6. Image analysis of PSI-200 top view projections. A gallery of 24 projections (out of 210) selected from digitized micrographs. Most projections have an egg-form with one edge more pointed than the other one. Inset: sum of 104 (out of 210) aligned projections. The field of the displayed sum is 27 × 27 nm, on the same scale as Fig. 3.

among the larger particles there is a quite homogeneous group which measures 20 × 16 nm in top view projection (Table I).

Image analysis was performed on 210 top-view projections selected from four digitized electron micrographs. After repeated alignments on improved references, starting with five different initial references, the 104 best aligned projections were summed (Fig. 6). This sum shows an averaged image with dimensions of 47 × 36 pixels or 19.8 × 15.1 nm, and these figures are close to the dimensions listed in Table I. After correction for the detergent boundary layer [23], the dimensions of PSI-200 would be about 16 × 12 nm. The averaged image is elongated and one of the two outer edges is slightly more pointed that the other one (Fig. 6). This feature can also be seen from the individual projections in the gallery of Fig. 6. This gallery and the sum also show that the projections are slightly asymmetrical as for CPI.

From Fig. 6 it is clear that there is a population of large PSI-200 complexes with an elongated shape. However, the inner density fluctuations of the top view projection are quite random and no subunit structures could be resolved. This is not unexpected, since uranyl acetate, the negative staining salt, generally is unable to penetrate hydrophobic structure parts.

Discussion

The dimensions and shapes of the different PS I preparations were determined by direct measurement from prints and from image analysis. The top-view dimensions determined from image analysis are slightly smaller for both CPI (15.2 × 9.7 nm) and PSI-200 (19.8 × 15.1 nm) projections. An identical small discrepancy was previously noticed for the 19 nm trimeric PS I particles [11], in which case direct measurements gave 20 nm for the diameter. It is evident that the detergent boundary layer around the proteins in top-view projection is the main factor limiting the accuracy of the measurements. Nevertheless, the set of measurements from Table I, in combination with subunit masses of the respective subunits, can be used for some calculations. The PSI-200 complex in the top view projection is about 77% larger than PSI-100 (Table I), and 110% larger if corrected for detergent. The increase in size is caused by attachment of LHCI complexes, which are absent for PSI-100. The PSI-200 complex from spinach has four different LHCI subunits [26,27] with molecular masses of 24–28 kDa determined on SDS-PAGE. The sequence of three of these genes has been determined for tomato [28–30] and from these sequences masses ranging between 22 and 26.1 kDa have been derived. One copy of each of the four LHCI subunits would increase the mass of a PSI-100 particle by about 47% (96 kDa) and two copies of each by about by 91%, assuming that all the intrinsic subunits have the same mass/volume ratio and that each LHCI monomer has about 12 attached Chl molecules. However, most of the smaller PS I subunits are largely or fully extrinsic, as has been predicted from their sequences [5–9,24]. Presumably, their contribution to the shape of the top-view projection of native PS I is smaller, as discussed previously. If we correct for this smaller contribution, two copies of each of the four

LHCI subunits would then enlarge the PSI-100 particle by about 100% in the top-view projection. This is quite close to the figure of 110%, which is the observed difference between the PSI-100 complex and the PSI-200 complex. If each LHCI binds approx. 12–13 chlorophyll molecules, and there are two copies each, then this would account for the 100 chlorophylls lost during the PSI-100 preparation as binding solely to the antenna peptides.

Recently the structure of LHCII trimers, interacting with PS II, and consisting of monomers of 25 kDa was determined at 0.37 nm resolution in projection [31]. The LHCII monomers have maximal overall dimensions of 2.4×4.4 nm in the plane of the membrane. LHCI and LHCII subunits have quite similar amino-acid compositions [32] and about the same mass. If the LHCI subunits have approximately the same shape, a shell of about eight subunits would cover the outer regions of the PSI-100 particle with its corrected dimensions of 7.7×12.8 nm, increasing the width and length of PSI-100 by about 4–5 nm. It is interesting to note that the PSI-100 and -200 preparations differ about 4–5 nm in both width and length. Moreover, they have some similarities in their shape: in both cases we found that the top view projection is elongated and that quite a number of projections have one of the two outer edges slightly more pointed than the other one (Figs. 5,6). These findings point to an arrangement of the LHCI monomers as depicted in the tentative model of Fig. 7. In this model no trimeric LHCI aggregates exist. Such trimers, which could exist in vivo for LHCII [31], have a diameter of over 6 nm and attachment of similar LHCI trimers to PSI-100 would give projections which differ in size and shape compared to the ones found for PSI-200.

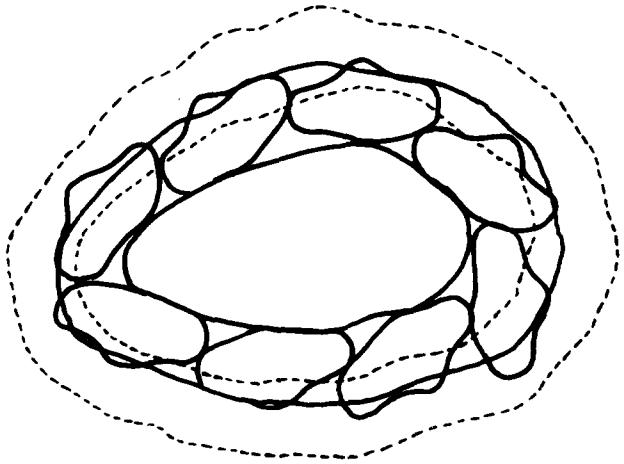

Fig. 7. A tentative model for the LHCI subunit arrangement in the PSI-200 complex from spinach, in which the core complex (PSI-100) is shown as enclosed in a shell of eight LHCI subunits. Dotted lines indicate the contours of the detergent complexes PSI-200 (Fig. 6) and of CPI (Fig. 3A). The latter class is shown both because its dimensions are very close to PSI-100, and because the images of PSI-100 could not be computer-analyzed to the same extent as those of CPI. The solid lines indicate the contours of both particles after correction for a detergent boundary layer of 1.7 nm (see text).

Results from freeze-fracture studies on pea chloroplast membranes grown under different light conditions [33] give some evidence for our model. It was found that the PS II reaction center complex is surrounded by discrete aggregates of LHCII subunits, giving rise to particles which differ by steps of about 2.5 nm [33], from 8 nm to 10.5 nm, 13.2 nm and 16.4 nm, respectively. These increments can be most easily realized by attachment of one (layer of) LHCII subunit(s), which have a width of 2.4 nm [31]. Probably, the LHCI subunits could surround the PSI-100 particles in a similar way, making them 2.5 nm thicker on one side, as depicted in the model.

The results of freeze-fracture studies on PS I indicate that the largest PS I complexes have a diameter of 13 nm [14,15]. This value is somewhat smaller than the 16×12 nm for our PSI-200 top view, but the difference is not of such a magnitude that it would make our model unlikely.

Acknowledgements

We wish to thank Prof. E.F.J. van Bruggen for general support, Dr. W. Keegstra for his help with computer image analysis, Mr. J. Haker for technical assistance and Mr. K. Gilissen for photography. This work was supported by grants from the Royal Netherlands Academy of Sciences (KNAW) to E.J.B. and the National Science Foundation to R.M.

References

1 Setif, P. and Mathis, P. (1986) in Photosynthesis III, Photosynthetic Membranes and Light Harvesting Systems (Staehelin, L.A. and Arntzen, C.J., eds.), pp. 476–486, Springer, Berlin.
2 Golbeck, J.H. (1987) Biochim. Biophys. Acta 895, 167–204.
3 Fish, L.E., Kuck, U. and Bogorad, L. (1985) J. Biol. Chemistry 260, 1413–1421.
4 Fish, L.E. and Bogorad, L. (1986) J. Biol. Chemistry 261, 8134–8139.
5 Lagoutte, B. (1988) FEBS Lett. 232, 275–280.
6 Okkels, J.S., Jepsen, L.B., Honberg, L.S., Lehmbeck, J., Scheller, H.V., Brandt, P., Hoyer-Hansen, G., Stummann, B., Henningsen, K.W., Von Wettstein, D. and Moller, B.L. (1988) FEBS Lett. 237, 108–112.
7 Steppuhn, J., Hermans, J., Nechustai, R., Ljungberg, U., Thümmler, F., Lottspeich, F. and Hermann, R.G. (1988) FEBS Lett. 237, 218–224.
8 Hayashida, N., Matsubayashi, T., Shinozaki, K., Sugiura, M., Inoue, K. and Hiyama, T. (1987) Curr. Genetics 12, 247–250.
9 Oh-oka, H., Takahashi, Y., Kuriyama, K. Saeki, K. and Matsubara, H. (1988) J. Biochem. 103, 962–968.
10 Boekema, E.J., Dekker, J.P., Van Heel, M.G., Rögner, M., Saenger, W., Witt, I. and Witt, H.T. (1987) FEBS Lett. 217, 283–286.
11 Boekema, E.J., Dekker, J.P., Rögner, M., Witt, I., Witt, H.T. and Van Heel, M. (1989) Biochim. Biophys. Acta 974, 81–87.
12 Ford, R.C. and Holzenburg, A. (1988) EMBO J. 7, 2287–2293.

13 Rögner, M., Mühlenhoff, U., Boekema, E.J. and Witt, H.T. (1990) Biochim. Biophys. Acta 1015, 415–424.
14 Dunahay, T. and Staehelin, L.A. (1985) Plant Physiol. 78, 606–613.
15 Staehelin, L.A. (1986) in Photosynthesis III, Photosynthetic Membranes and Light Harvesting Systems (Staehelin, L.A. and Arntzen, C.J., eds.), pp. 1–84, Springer, Berlin.
16 Simpson, D.J. (1983) Eur. J. Cell Biol. 31, 305–314.
17 Wynn, R.M. and Malkin, R. (1988) Biochemistry 27, 5863–5869.
18 Van Heel, M.G. and Keegstra, W. (1981) Ultramicroscopy 7, 113–130.
19 Boekema, E.J., Berden, J.A. and Van Heel, M.G. (1986) Biochim. Biophys. Acta 851, 353–360.
20 Harauz, G., Boekema, E.J. and Van Heel, M. (1988) Methods Enzymol. 164, 35–49.
21 Van Heel, M.G. and Frank, J. (1981) Ultramicroscopy 6, 187–194.
22 Bijlholt, M.M.C., Van Heel, M.G. and Van Bruggen, E.F.J. (1982) J. Mol. Biol. 161, 139–153.
23 Timmins, P.A., Leonhard, M., Weltzien, H.U., Wacker, T. and Welte, W. (1988) FEBS Lett. 238, 361–368.
24 Moller, B.L., Scheller, H.V., Okkels, J.S., Jepsen, L.B., Koch, B., Andersen, B. and Hoj, P.B. (1989) Physiol. Plant. 76, A24.
25 Andreasson, E., Svensson, P., Weibull, C. and Albertsson, P.A. (1988) Biochim. Biophys. Acta 936, 339–350.
26 Lam, E., Ortiz, W., Mayfield, S. and Malkin, R. (1984) Plant Physiol. 74, 650–655.
27 Lam, E., Ortiz, W. and Malkin, R. (1984) FEBS Lett. 168, 10–14.
28 Hofman, N.E., Pichersky, E., Malik, V.S., Castresana, C., Ko, K., Darr, S. and Cashmore, A.R. (1987) Proc. Natl. Acad. Sci. USA 84, 8844–8848.
29 Pichersky, E., Tanksley, S.D., Piechulla, B., Stayton, M.M. and Dunsmuir, P. (1988) Plant Mol. Biol. 11, 69–71.
30 Pichersky, E., Brock, T.G., Nguyen, D., Hoffman, N.E., Piechulla, B., Tanksley, S.D. and Green, B. (1989) Plant Mol. Biol. 12, 257–270.
31 Kühlbrandt, W. and Downing, K.H. (1989) J. Mol. Biol. 207, 823–828.
32 Nechustai, R., Peterson, C.C., Peter, G.F. and Thornber, J.F. (1987) Eur. J. Biochem. 164, 345–350.
33 Armond, P.A., Staehelin, L.A. and Arntzen, C.J. (1977) J. Cell Biol. 73, 400–418.